




 Cite this: *New J. Chem.*, 2022, **46**, 15495

# A carbon nanowire-promoted Cu<sub>2</sub>O/TiO<sub>2</sub> nanocomposite for enhanced photoelectrochemical performance

 Kassam Ahmed,<sup>a</sup> Yuyin Wang,<sup>b</sup> Yang Bai,<sup>b</sup> Karthikeyan Sekar <sup>\*c</sup> and Wei Li <sup>\*b</sup>

The use of semiconductors as photoelectrochemical electrodes and photocatalysts has been studied extensively over the last few decades; however, it is challenging to design one single material meeting a wide range of requirements for applications such as photostability, wide light absorbance and earth abundance. In this study, we started with earth-abundant materials, namely TiO<sub>2</sub>, Cu<sub>2</sub>O and carbon, to design a nanocomposite with TiO<sub>2</sub> nanofibers (NFs) and Cu<sub>2</sub>O nanocubes (NCs) connected by carbon nanowires (NWs). The nanocomposite (C/TiO<sub>2</sub>/Cu<sub>2</sub>O) demonstrated excellent photo(electro)activity under simulated visible light as well as enhanced durability. Morphologies imaged by electron microscopes showed that TiO<sub>2</sub> NFs and Cu<sub>2</sub>O NCs were well connected, while thin and long carbon NWs were present throughout the samples and connected the NFs and NCs to form a compact composite. Electrochemical analysis revealed that the band alignment between TiO<sub>2</sub> and Cu<sub>2</sub>O was typical for a type-II heterojunction, which is favourable for the separation of photogenerated charge carriers. Moreover, carbon NWs act as bridges, thus facilitating more efficient charge transfer. Overall, this research showed the design and preparation of a nanostructured composite with improved charge transfer and photostability for solar photoelectrochemical applications.

 Received 23rd June 2022,  
 Accepted 11th July 2022

DOI: 10.1039/d2nj03116g

[rsc.li/njc](http://rsc.li/njc)

## 1. Introduction

Technologies based on photon and semiconductor interactions, *e.g.* photoelectrochemical and photocatalysis water splitting, have become attractive research areas in recent decades because they can offer a sustainable roadmap towards clean fuels and the environment. An important factor for advancing the research is to obtain catalytic/electrode materials with suitable properties, such as wide light absorbance, photostability, high efficiency, environment friendliness and earth abundance. An extensive range of materials have been studied over the last few decades,<sup>1–10</sup> but each has its own limitations.<sup>11–15</sup>

Titanium dioxide (TiO<sub>2</sub>) is a well-known stable n-type semiconductor used over the last few decades with a large band gap of 3.2 eV;<sup>11</sup> thus, it is mainly active in the ultraviolet (UV) region, which is only 4% of the solar spectrum. Efforts have been devoted to expanding the spectral response of TiO<sub>2</sub> in the visible light region using various band engineering methods,

such as surface modification, metal doping, creating heterojunction, co-catalyst loading and coupling with narrow band gap semiconductors.<sup>16</sup>

A highly attractive narrow band gap semiconductor, Cu<sub>2</sub>O, is found in abundant, low-cost and non-toxic p-type semiconductor with a band gap between 2.0 and 2.2 eV.<sup>17</sup> However, Cu<sub>2</sub>O is prone to photocorrosion, which is attributed to the oxidation and reduction potential of Cu<sub>2</sub>O lying within the band gap.<sup>18</sup>

TiO<sub>2</sub>–Cu<sub>2</sub>O as a binary heterojunction/composite has demonstrated synergistic photoelectrochemical and photocatalytic performance based on efficiency and stability.<sup>19</sup> However, there are inevitable defects or poor connections at the interface between the two different components, which act as charge carrier sinks and hinder efficient charge carrier migration. A strategy to improve the interface and provide better connections between the two different components is highly desirable to fully unleash the synergy between TiO<sub>2</sub> and Cu<sub>2</sub>O, thus providing an ideal catalyst for photoelectrochemical and photocatalytic applications.

There are attempts to utilise carbon nanomaterials in composite photoelectrochemical electrode materials and photocatalysts as charge transfer promoters and structure stabilisers. For example, carbon nanowires (NWs) are known to have excellent mechanical and electron transport properties.<sup>20</sup>

In addition to the physical and chemical properties of TiO<sub>2</sub> and Cu<sub>2</sub>O, their structural properties (*e.g.* morphology, surface

<sup>a</sup> School of Engineering and Applied Science, Aston University, Birmingham B4 7ET, UK

<sup>b</sup> Institute for Materials and Processes, School of Engineering, University of Edinburgh, Mayfield Road, Edinburgh EH9 3JL, UK. E-mail: wei.li@ed.ac.uk

<sup>c</sup> Department of Chemistry, SRM Institute of Science and Technology, Kattankulathur, Tamil Nadu, India. E-mail: karthik.keyan02@gmail.com



area and crystallinity) also play vital roles in their photoelectrochemical and photocatalytic properties. In our previous study, it is already revealed that high crystalline TiO<sub>2</sub> nanofibers (NFs) and Cu<sub>2</sub>O nanocubes (NCs) can offer optimised charge transfer efficiency and photostability compared to other structures.<sup>19,21–23</sup>

In this study, we designed a nanocomposite with TiO<sub>2</sub> NFs and Cu<sub>2</sub>O NCs, which was further connected and enhanced by carbon NWs. The synthesis procedure was simple and required inexpensive solvents and operating conditions. The photoelectrochemical (PEC) performance of the ternary C-NW/TiO<sub>2</sub> NF/Cu<sub>2</sub>O composite showed improved charge carrier separation, superior PEC activity and enhanced stability.

## 2. Experimental

### 2.1. Synthesis of C-NW/TiO<sub>2</sub> NF

A single crystalline 1D TiO<sub>2</sub> NF was fabricated as described in our previous study *via* topotactic transformation by ion-exchange and dehydration.<sup>22</sup> Subsequent C-NW/TiO<sub>2</sub> NF was prepared by a hydrothermal synthesis using gelatine as the carbon precursor as it is a cheap polymer obtained from animal skin, bones and tissues.<sup>24</sup> It is known to have strong coating interactions with metal nanoparticles.<sup>25</sup> Gelatine was dissolved in a mixture of TiO<sub>2</sub> NFs in 20 ml water and stirred at 40 °C. The sample was placed in a stainless-steel autoclave and heated at 250 °C for 4 h. After the hydrothermal treatment, the sample was centrifuged at 7000 rpm for 10 min with several washes of water and dried in the oven. Gelatine is abundant in amino and carboxyl groups, so it can be hydrothermally treated with only pure water. Hence, it is an inexpensive water-soluble polymer. An advantage of this procedure is that no strong acid or surface passivation reagent or post-treatment is needed to fabricate C-NW/TiO<sub>2</sub> NFs.<sup>26</sup>

### 2.2. Synthesis of C-NW/TiO<sub>2</sub> NF/Cu<sub>2</sub>O

C-NW/TiO<sub>2</sub> NF/Cu<sub>2</sub>O was synthesised by solution phase chemistry under ambient conditions, as described previously.<sup>16</sup> The TiO<sub>2</sub> to Cu<sub>2</sub>O ratio was targeted at 1:1 by controlling the dosages of corresponding precursors in the synthesis process. In a typical process, PEG was ultrasonicated in 100 ml of water for 30 min. C-NW/TiO<sub>2</sub> NF was mixed with 0.2 M CuCl<sub>2</sub> and 0.01 M PEG-600 before ultrasonication for 10 min. This mixture was then heated to 50 °C, forming a blue solution. 2 M NaOH was poured into the blue solution and 0.2 M N<sub>2</sub>H<sub>4</sub>·H<sub>2</sub>O was added dropwise in the stirred mixture to generate Cu(I) ions and further heated for 10 min. The resulting mixture was purged in N<sub>2</sub> to form C-NW/TiO<sub>2</sub> NF/Cu<sub>2</sub>O, followed by centrifugation at 7000 rpm with several washes with H<sub>2</sub>O and ethanol to remove any residual PEG.

### 2.3. Characterisation methods

TEM images were taken at 200 kV on a JEM-2100Plus microscope (Warwick University, UK). Samples were prepared by ultrasonication and drop-casted on a Cu grid coated with a carbon film. Powder X-ray diffraction (XRD) was operated on a Bruker-AXS D8 ADVANCE diffractometer at 40 kV, 40 mA and

Cu K $\alpha$  radiation ( $\lambda = 0.15418$  nm) between  $2\theta$  10 and 80° in 0.02° steps. Brunauer–Emmett–Teller (BET) surface areas were calculated at 77 K by N<sub>2</sub> physisorption using a Quantachrome NOVA 4000e porosimeter on degassed samples at 120 °C for 4 h. Diffuse reflectance UV-Vis Spectra (DRUVS) were recorded on a Thermo Scientific Evo220 Spectrometer using KBr as a standard in an absorbance range between 200 and 700 nm. The ratio of TiO<sub>2</sub> to Cu<sub>2</sub>O in TiO<sub>2</sub> NF/Cu<sub>2</sub>O and C-NW/TiO<sub>2</sub> NF/Cu<sub>2</sub>O samples was quantified by ICP-OES (Optima2000DV, USA).

### 2.4. Photoelectrochemical methods

A homogenous colloid was formed within 30 min of sonication of the as-prepared samples (5 mg), and Nafion (10  $\mu$ L, 5 wt%) was dispersed in a water/ethanol mixture (1 ml, 3:1 v/v). 5  $\mu$ L colloid was deposited on a glassy carbon electrode (3 mm dia.) used as the working electrode. A Pt wire was used as the counter electrode, and Hg/Hg<sub>2</sub>SO<sub>4</sub> was used as the reference electrode in a three-electrode photoelectrochemical cell. The electrolyte (0.5 M Na<sub>2</sub>SO<sub>4</sub>) was purged in N<sub>2</sub> for 30 min. A 200 W Hg–Xe arc lamp (Oriel Instruments 66002, with UV cutoff filter,  $\lambda > 420$  nm) was used as the light source. The light intensity was adjusted and kept at 100 mW cm<sup>-2</sup> for all experiments. Measurements were performed using Autolab potentiostat with Nova software. Mott–Schottky plots were recorded under DC polarisation at a potential range of -1 to 0 V with a potential step of 10 mV at a frequency of 1000 Hz. Nyquist plots were recorded under an AC signal of 10 mV at a frequency range of 100 kHz–0.1 Hz.

## 3. Results and discussion

TEM and SEM images in Fig. 1 show the morphology and size of the individual components and C-NW/TiO<sub>2</sub> NF/Cu<sub>2</sub>O as a

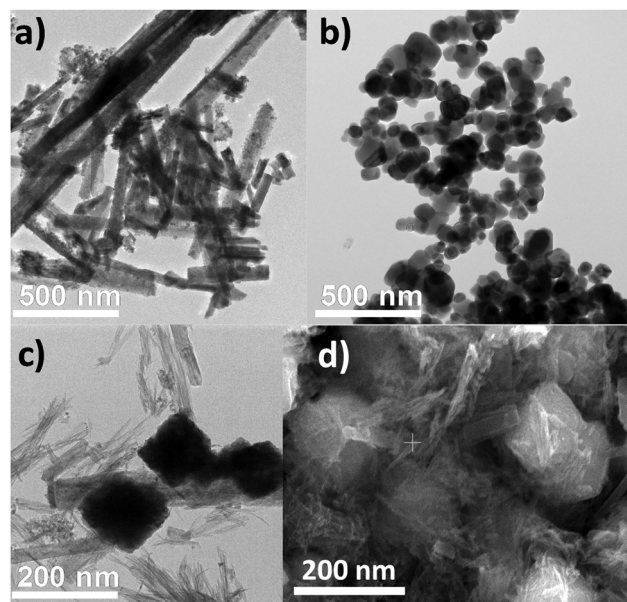


Fig. 1 TEM images of (a) TiO<sub>2</sub> NF, (b) Cu<sub>2</sub>O nanocubes, (c) C-NW/TiO<sub>2</sub> NF/Cu<sub>2</sub>O, and (d) SEM images of C-NW/TiO<sub>2</sub> NF/Cu<sub>2</sub>O.



nanocomposite. Fig. 1a demonstrates the 1D TiO<sub>2</sub> NF with lengths between 500 nm and 5 μm and diameters between 100 and 200 nm. Fig. 1b illustrates the Cu<sub>2</sub>O nanocubes with sizes ranging between 150 and 250 nm. After the hydrothermal synthesis, amino acids were carbonised to form carbon NWs, and thus the ternary Cu<sub>2</sub>O, C-NW and TiO<sub>2</sub> nanocomposite was formed, as shown in Fig. 1c and d. In these two images, cubic Cu<sub>2</sub>O, TiO<sub>2</sub> NF and C-NW were all clearly visible. TiO<sub>2</sub> NFs were intimately in contact with Cu<sub>2</sub>O nanocubes, with C-NWs occupying the spaces and further promoting the Cu<sub>2</sub>O–TiO<sub>2</sub> connections.

XRD patterns confirmed the characteristics of Cu<sub>2</sub>O and TiO<sub>2</sub> peaks in Fig. 2a, indicating that the heterojunction nanocomposite consists of Cu<sub>2</sub>O and TiO<sub>2</sub>, which is in good agreement with the TEM and SEM images. The diffraction peaks for TiO<sub>2</sub> NF were well defined and corresponded to the crystal planes of (101), (004), (200), (105), (211) and (204) at  $2\theta = 25.3^\circ, 37.8^\circ, 48.0^\circ, 53.8^\circ, 55.4^\circ$  and  $62.5^\circ$ , respectively, which confirmed anatase TiO<sub>2</sub> NF (tetragonal, JCPDS 21-1272).<sup>27</sup> The XRD patterns illustrated the formation of crystalline Cu<sub>2</sub>O by  $2\theta$  peaks at  $29.6^\circ, 36.4^\circ, 42.3^\circ, 61.4^\circ, 73.5^\circ$  and  $77.4^\circ$ , which are associated with characteristic (110), (111), (200), (220), (311), and (222) peaks of Cu<sub>2</sub>O, respectively (cubic, JCPDS 73-0687).<sup>28</sup> The ratio of TiO<sub>2</sub> to Cu<sub>2</sub>O in TiO<sub>2</sub> NF/Cu<sub>2</sub>O and C-NW/TiO<sub>2</sub> NF/Cu<sub>2</sub>O samples was quantified as 0.9:1 by ICP-OES. There were weak traces of CuO in both Cu<sub>2</sub>O and TiO<sub>2</sub> NF/Cu<sub>2</sub>O, which is in agreement with JCPDS 45-0937<sup>29</sup> but not observed in the C-NW/TiO<sub>2</sub> NF/Cu<sub>2</sub>O sample. There is a weak but a broad pattern at  $25^\circ$ , suggesting either a low concentration of C-NWs or the amorphous carbon.

The carbon content in C-NW/TiO<sub>2</sub> NF/Cu<sub>2</sub>O was investigated by thermogravimetric analysis (TGA), as shown in Fig. 2b. There are three significant weight losses at 100 °C, 200 °C and 400 °C, respectively. The initial loss for the samples at 100 °C was due to the adsorbed moisture (2.1%), while the 2.9% weight loss until 200 °C was attributed to the removal of residual PEG, which was the structuring agent used to fabricate Cu<sub>2</sub>O

nanocubes. The weight loss above 200 °C was 4.3%, which accounted for the total loss of C-NWs in the heterojunction. Different C-NW contents (*i.e.*, in the range from 2% to 10%) were prepared. Within this range, there was no clear difference in various photoelectrochemical performances. This 4.3% sample was presented as a representative. Fig. 2c illustrates the nature of carbon in C-NW/TiO<sub>2</sub> NF/Cu<sub>2</sub>O using Raman spectroscopy. The Raman spectrum shows two peaks of  $1370\text{ cm}^{-1}$  and  $1593\text{ cm}^{-1}$  for the D and G bands, respectively, which is characteristic of amorphous carbon.

Surface areas varied between the different samples (Fig. 2d), with Cu<sub>2</sub>O nanocubes having the lowest BET surface area of  $22.9\text{ m}^2\text{ g}^{-1}$ . TiO<sub>2</sub> NF exhibited the highest BET surface area of  $93.5\text{ m}^2\text{ g}^{-1}$ . Binary TiO<sub>2</sub> NF/Cu<sub>2</sub>O had a surface area of  $53.8\text{ m}^2\text{ g}^{-1}$  reasonably between the two individual components. C-NW/TiO<sub>2</sub> NF/Cu<sub>2</sub>O had a higher BET surface area than TiO<sub>2</sub> NF/Cu<sub>2</sub>O, which was due to the integration of C-NWs as it has a high surface area. This may have further implications for photoelectrochemical performance because C-NWs may act as an electron anchor by improving electron mobility and transportation in the heterojunction.<sup>30,31</sup>

The optical properties of different samples were analysed and presented in Fig. 3, whereby the absorbance spectra ranged from 200 to 600 nm (Fig. 3a), consistent with previously reported.<sup>32</sup>

The optical band gaps  $E_{\text{BG}}$  were calculated from the Tauc plots (Fig. 3b) using eqn (1).

$$\alpha h\nu = C(h\nu - E_{\text{BG}})^n \quad (1)$$

where  $C$  is the proportionality constant and ' $\alpha$ ' is the absorption coefficient determined from the Kubelka–Munk formula (eqn (2)).

$$\alpha = \frac{(1 - R)^2}{2R} \quad (2)$$

The direct band gaps of TiO<sub>2</sub> NF, Cu<sub>2</sub>O, TiO<sub>2</sub> NF/Cu<sub>2</sub>O and C-NW/TiO<sub>2</sub> NF/Cu<sub>2</sub>O were 3.28, 2.36, 2.38 and 2.21 eV, respectively, as presented in Table 1. The tested samples containing

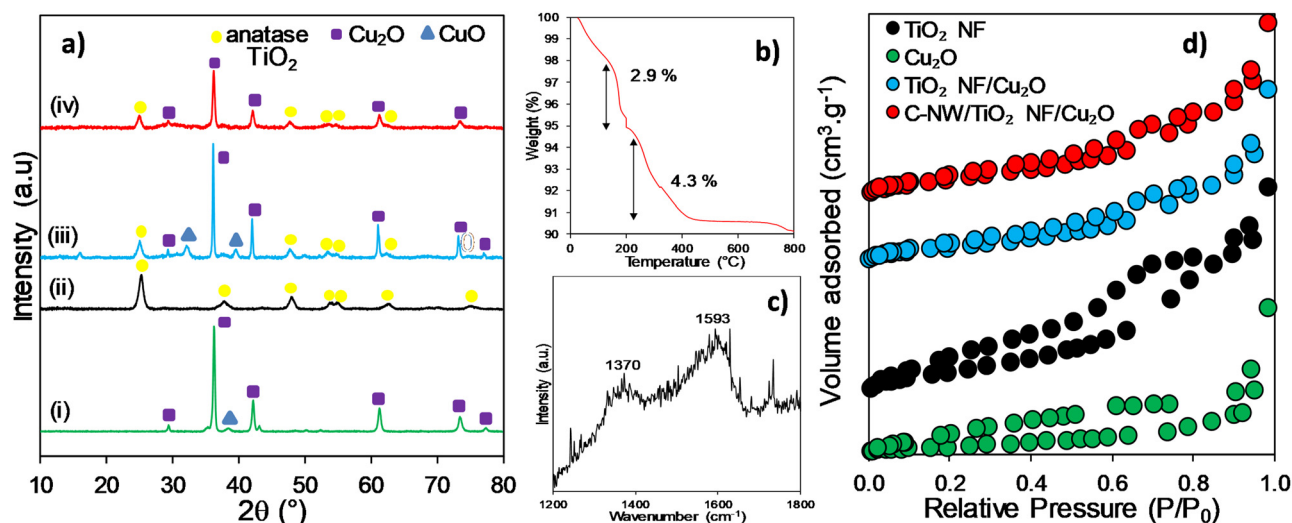


Fig. 2 (a) XRD patterns of (i) Cu<sub>2</sub>O, (ii) TiO<sub>2</sub> NF, (iii) TiO<sub>2</sub> NF/Cu<sub>2</sub>O and (iv) C-NW/TiO<sub>2</sub> NF/Cu<sub>2</sub>O. (b) TGA and (c) Raman spectrum of C-NW/TiO<sub>2</sub> NF/Cu<sub>2</sub>O. (d) N<sub>2</sub> adsorption–desorption isotherms of TiO<sub>2</sub> NF, Cu<sub>2</sub>O nanocubes, TiO<sub>2</sub> NF/Cu<sub>2</sub>O, C-NW/TiO<sub>2</sub> NF/Cu<sub>2</sub>O.



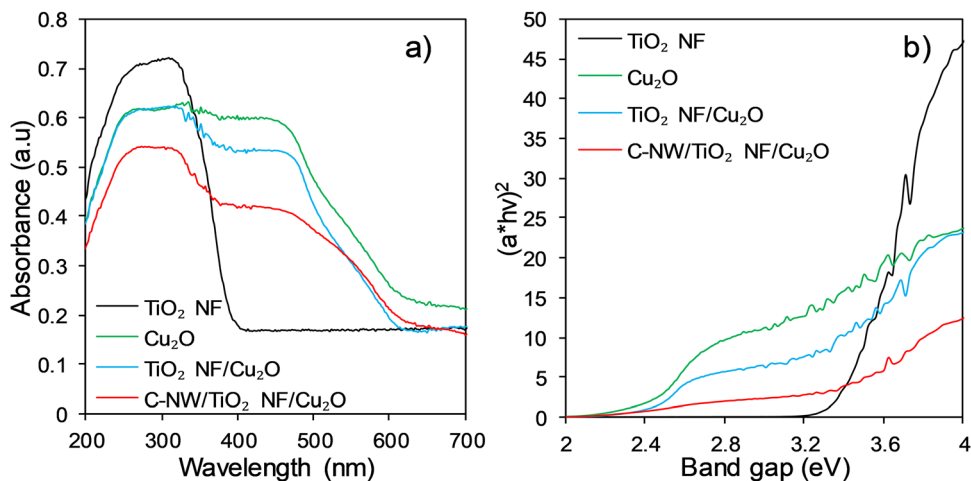


Fig. 3 (a) DRUVS and (b) Tauc plots of  $\text{TiO}_2$  NF,  $\text{Cu}_2\text{O}$ ,  $\text{TiO}_2$  NF/ $\text{Cu}_2\text{O}$  and C-NW/ $\text{TiO}_2$  NF/ $\text{Cu}_2\text{O}$ .

Table 1 Photophysical properties of  $\text{TiO}_2$  NF,  $\text{Cu}_2\text{O}$ ,  $\text{TiO}_2$  NF/ $\text{Cu}_2\text{O}$  and C-NW/ $\text{TiO}_2$  NF/ $\text{Cu}_2\text{O}$

Sample	BET surface area <sup>a</sup> ( $\text{m}^2 \text{g}^{-1}$ )	Band gap <sup>b</sup> (eV)
$\text{TiO}_2$ NF	93.5	3.28
$\text{Cu}_2\text{O}$	22.9	2.36
$\text{TiO}_2$ NF/ $\text{Cu}_2\text{O}$	53.8	2.38
C-NW/ $\text{TiO}_2$ NF/ $\text{Cu}_2\text{O}$	66.9	2.21

<sup>a</sup>  $\text{N}_2$  porosimetry. <sup>b</sup> DRUVS.

$\text{Cu}_2\text{O}$  absorbed light in the visible region at the wavelength of 650 nm. Two absorbance peaks are present at 300 nm and 480 nm, confirming both components were present in the system, which is in agreement with a previous report.<sup>33</sup> C-NW/ $\text{TiO}_2$  NF/ $\text{Cu}_2\text{O}$  showed a red shift to  $\text{TiO}_2$  NF/ $\text{Cu}_2\text{O}$ , which indicates C-NWs have strong visible light absorption properties. It may also promote interfacial contact between C-NWs and the two semiconductors.

The effect of C-NW enhancement on the interfacial charge transfer between the  $\text{TiO}_2$  NF- $\text{Cu}_2\text{O}$  heterojunction was investigated using PEC measurements under chopped visible light illumination at 0 V vs. RHE. PEC measurements were studied in a three-electrode system, with Pt wire as the counter electrode,  $\text{Hg}/\text{Hg}_2\text{SO}_4$  as the reference electrode, and different samples were drop-casted onto a glassy carbon electrode as the working electrode. Fig. 4a shows C-NW/ $\text{TiO}_2$  NF/ $\text{Cu}_2\text{O}$  >  $\text{TiO}_2$  NF/ $\text{Cu}_2\text{O}$  >  $\text{Cu}_2\text{O}$  >  $\text{TiO}_2$  NF in terms of photoresponse. In order to enable comparison with other reported and relevant  $\text{TiO}_2$ -based materials, the widely used benchmark P25  $\text{TiO}_2$  was also tested, showing photoresponse similar to  $\text{TiO}_2$  NF (data did not show as it overlapped with that of  $\text{TiO}_2$  NF), which was consistent with our previous study.<sup>19</sup> The low photocurrent density of  $\text{TiO}_2$  NF was attributed to poor visible light response, and  $\text{Cu}_2\text{O}$  had photostability issues during charge transfer. The photocurrent density of C-NW/ $\text{TiO}_2$  NF/ $\text{Cu}_2\text{O}$  was approximately 6 times higher than  $\text{TiO}_2$  NF/ $\text{Cu}_2\text{O}$  and above the factor of 8 times higher than both  $\text{Cu}_2\text{O}$  and  $\text{TiO}_2$  NF. The C-NW promoted the heterojunction nanocomposite produced a higher photocurrent response,

indicating more efficient charge transfer, where C-NWs can act as a carrier mobility layer at the  $\text{TiO}_2$  NF/ $\text{Cu}_2\text{O}$  interface.<sup>34</sup>  $\text{Cu}_2\text{O}$  was difficult to use in practical applications as it has low photostability; therefore, the impact of C-NWs on catalyst stability (Fig. 4b) was studied. The photocurrent generated by  $\text{Cu}_2\text{O}$  decreased at a faster rate than C-NW/ $\text{TiO}_2$  NF/ $\text{Cu}_2\text{O}$  over a time period of 24 hours, which suggests that the addition of  $\text{TiO}_2$  NF and C-NWs increased photostability. The advantage of C-NW as a conductive network was more profound when we consider that the samples were dropcasted on a glassy carbon electrode. The sample particles formed a dense layer with the C-NW conductive network embedded, which could not only promote the charge mobility but also enhance the  $\text{Cu}_2\text{O}$  stability.

Bare  $\text{TiO}_2$  NF showed a low photocurrent density vs. voltage curves (Fig. 4c), but  $\text{Cu}_2\text{O}$  nanocubes exhibited a higher photocurrent density under visible light due to its narrow band gap. With the introduction of the heterojunction nanocomposite,  $\text{TiO}_2$  NF/ $\text{Cu}_2\text{O}$ , the photocurrent density increased to  $60.3 \mu\text{A cm}^{-2}$  at 1.23 V vs. RHE. The integration of C-NWs yielded a significant increase in the photocurrent density of  $139.8 \mu\text{A cm}^{-2}$ , which was almost 4 times higher than  $\text{TiO}_2$  NF. The sharp increase in the photocurrent density indicates high charge transfer and separation efficiency with C-NWs in C-NW/ $\text{TiO}_2$  NF/ $\text{Cu}_2\text{O}$ .<sup>35</sup> The results were similar in the chopped photocurrent density vs. voltage curve, as shown in Fig. 4d, where C-NW/ $\text{TiO}_2$  NF/ $\text{Cu}_2\text{O}$  reached photocurrent densities of  $122.4 \mu\text{A cm}^{-2}$  at  $-0.3$  V vs. RHE, which was 2 times higher than  $\text{TiO}_2$  NF/ $\text{Cu}_2\text{O}$ .

The interfacial properties of C-NW/ $\text{TiO}_2$  NF/ $\text{Cu}_2\text{O}$  were further studied by electrochemical impedance spectroscopy (EIS) in the form of a Nyquist plot. A Nyquist plot was used to investigate the characteristics of the charge transfer process, whereby the semicircle diameter indicates the charge transfer resistance. In Fig. 5a, the semicircle diameter of  $\text{Cu}_2\text{O}$  and  $\text{TiO}_2$  NF is slightly larger than that of  $\text{TiO}_2$  NF/ $\text{Cu}_2\text{O}$ , which shows they have similar charge transfer resistance. C-NW/ $\text{TiO}_2$  NF/ $\text{Cu}_2\text{O}$  exhibited the lowest charge transfer resistance, which is attributed to the integration of C-NWs. This indicates that C-NWs reduced the resistance to charge carrier transport due to





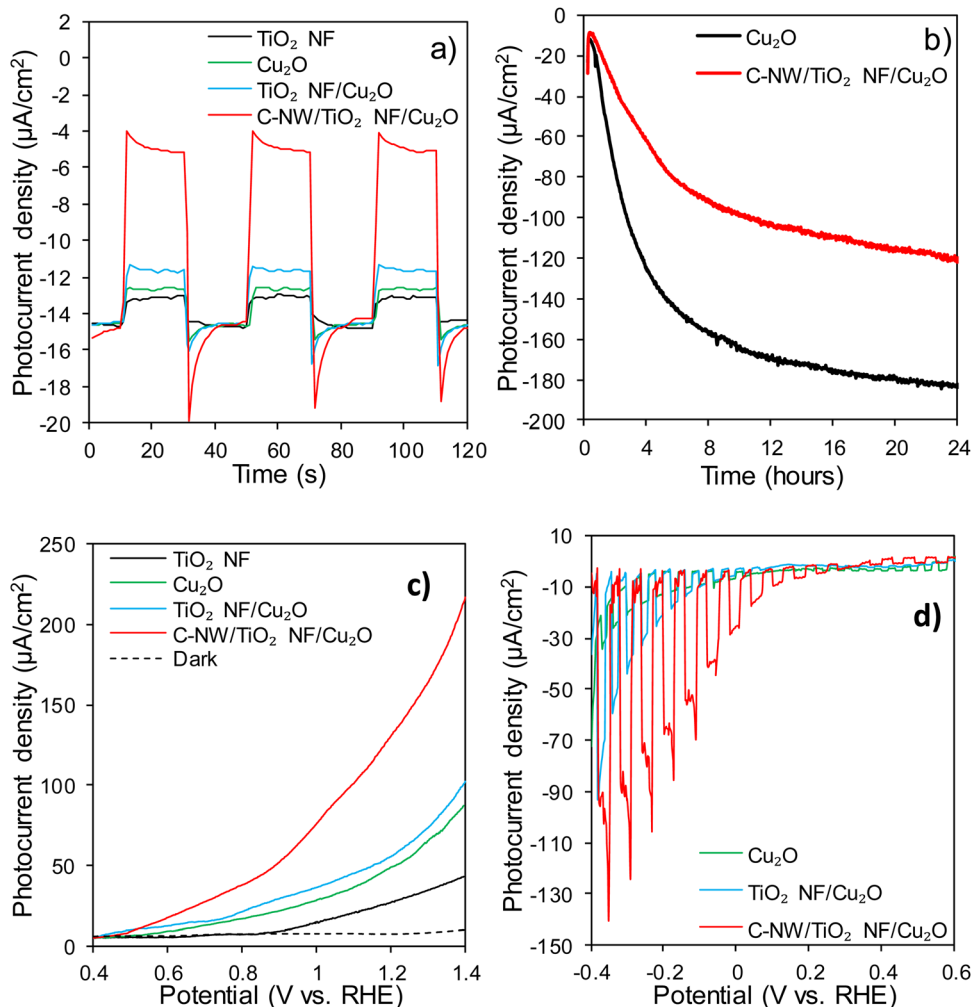


Fig. 4 (a) Transient photocurrent and (b) photostability (0 V vs. RHE) of TiO<sub>2</sub> NF, Cu<sub>2</sub>O, TiO<sub>2</sub> NF/Cu<sub>2</sub>O and C-NW/TiO<sub>2</sub> NF/Cu<sub>2</sub>O under visible light irradiation. (c) *I*–*V* curve and (d) chopped *I*–*V* curves of TiO<sub>2</sub> NF, Cu<sub>2</sub>O, TiO<sub>2</sub> NF/Cu<sub>2</sub>O and C-NW/TiO<sub>2</sub> NF/Cu<sub>2</sub>O under visible light irradiation at a scan rate of 10 mV s<sup>-1</sup>, (reaction conditions: 200 W Hg–Xe arc lamp, 0.5 M Na<sub>2</sub>SO<sub>4</sub> electrolyte).

the efficient separation of charge carriers in the nanocomposite.<sup>35</sup> Fig. 5b and c show the Mott–Schottky plots of TiO<sub>2</sub> NF, C-NW/TiO<sub>2</sub> NF and Cu<sub>2</sub>O, which were utilised to calculate the flat band potential and majority carrier densities of each semiconductor in the heterojunction. The positive and negative slopes are indicative of n-type and p-type semiconductors, respectively. This type of p–n heterojunction is a favourable structure for enhanced charge separation.<sup>36</sup> The flat band potentials are shown by the x-intercept of the linear section, which are -0.76 V, -0.72 V and 0.54 V, vs. RHE for TiO<sub>2</sub> NF, C-NW/TiO<sub>2</sub> NF and Cu<sub>2</sub>O, respectively. The anodic shift of 40 mV between TiO<sub>2</sub> NF and C-NW/TiO<sub>2</sub> NF is in agreement with previous reports.<sup>37</sup>

The gradient of the linear portion of the plot was used to calculate the majority carrier density ( $N_A$ ) calculated from eqn (3).

$$\frac{1}{C^2} = \frac{2}{\epsilon\epsilon_0 e N_A} \left( V - E_{fb} - \frac{k_B T}{e} \right) \quad (3)$$

where  $C$  is the capacitance,  $\epsilon$  is the dielectric constant of TiO<sub>2</sub> and Cu<sub>2</sub>O, which is 170<sup>38</sup> and 7.60,<sup>39</sup> respectively,  $\epsilon_0$  is the

permittivity of free space,  $V$  is the applied potential,  $E_{fb}$  is the flat band potential,  $e$  is the electron charge,  $k_B$  is the Boltzmann's constant and  $T$  is the temperature. The  $N_A$  values of Cu<sub>2</sub>O, TiO<sub>2</sub> NF and TiO<sub>2</sub> NF/C-NWs were  $5.36 \times 10^{18}$  cm<sup>-3</sup>,  $1.06 \times 10^{19}$  cm<sup>-3</sup> and  $1.30 \times 10^{19}$  cm<sup>-3</sup>, respectively. This showed that 1D TiO<sub>2</sub> NF had more charge carrier activity, but more studies are needed to gain conclusive results.

The valence band edge of Cu<sub>2</sub>O,  $E_V$ , was calculated from eqn (4):

$$E_V = E_F - k_B T \ln \frac{N_V}{N_A} \quad (4)$$

where the effective density of states,  $N_V = 2 \left( \frac{2\pi m_h k_B T}{h^2} \right)^{\frac{3}{2}}$ . The effective hole mass is denoted as  $m_h = 0.58m_e$  for Cu<sub>2</sub>O,<sup>40</sup> where  $m_e$  is the mass of a free electron.  $N_V$  for Cu<sub>2</sub>O was  $1.10 \times 10^{19}$  cm<sup>-3</sup>. The valence band edge ( $E_V$ ) was 0.56 V for Cu<sub>2</sub>O. Thus, as Cu<sub>2</sub>O has a band gap of 2.36, the valence and conduction band positions were at 0.56 V and -1.80 V vs. RHE,



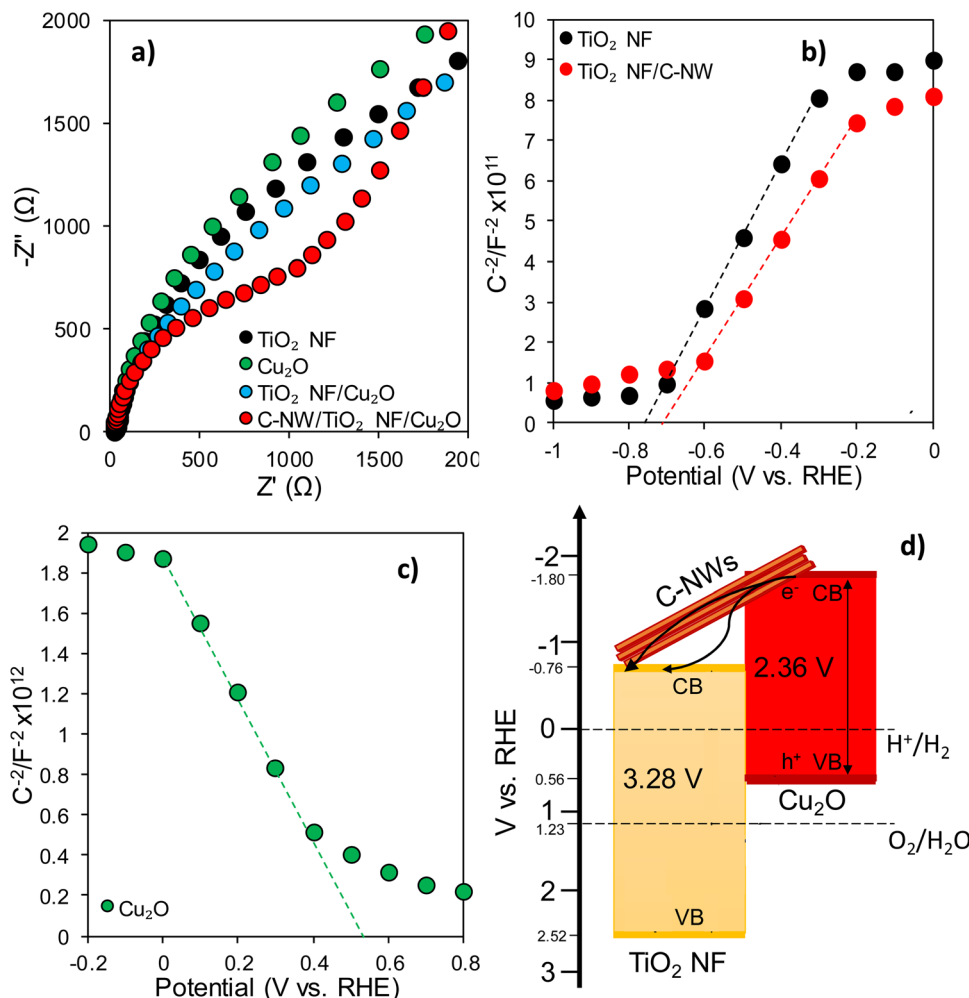


Fig. 5 (a) EIS (Nyquist plot at 0 V vs. RHE) of  $\text{TiO}_2$  NF,  $\text{Cu}_2\text{O}$ ,  $\text{TiO}_2$  NF/ $\text{Cu}_2\text{O}$  and C-NW/ $\text{TiO}_2$  NF/ $\text{Cu}_2\text{O}$  under visible light irradiation; Mott-Schottky plot of  $\text{TiO}_2$  NF (b) and  $\text{Cu}_2\text{O}$  (c); (200 W Hg-Xe arc lamp, 0.5 M  $\text{Na}_2\text{SO}_4$  electrolyte); (d) Schematic for the energy band structure of C-NWs/ $\text{TiO}_2$ / $\text{Cu}_2\text{O}$  nanocomposite.

respectively. Assuming the distance between the flat band potential of  $\text{TiO}_2$  NF and the lowest potential of the conduction band (CB) is negligible,<sup>40</sup> the CB of  $\text{TiO}_2$  NF was  $-0.76$  V vs. RHE. Thus, the band gap of  $\text{TiO}_2$  NF was 3.28, so the valence band and conduction band were positioned at 2.52 V and  $-0.76$  V vs. RHE, respectively.

A schematic of the energy band structure is proposed in Fig. 5d. The enhanced photoelectrochemical performance of C-NW/ $\text{TiO}_2$  NF/ $\text{Cu}_2\text{O}$  nanocomposite was attributed to a few reasons. As  $\text{Cu}_2\text{O}$  has a narrow bandgap energy of 2.36 eV, it can be excited by visible light. The conduction band of  $\text{TiO}_2$  lies at a more positive potential than that of  $\text{Cu}_2\text{O}$ , and the electrons from  $\text{Cu}_2\text{O}$  can inject into the conduction band of  $\text{TiO}_2$ . This prevents the recombination of photogenerated electrons and holes in  $\text{Cu}_2\text{O}$ .<sup>41</sup> Accumulated electrons in the conduction band of  $\text{TiO}_2$  can then transfer to the glassy carbon electrode.<sup>42</sup> The addition of C-NWs further broadens the solar absorption to the visible light region. Also, the impedance spectra show that the C-NW/ $\text{TiO}_2$  NF/ $\text{Cu}_2\text{O}$  nanocomposite has improved charge carrier density and least charge transfer

resistance compared to bare  $\text{TiO}_2$  NF and  $\text{Cu}_2\text{O}$ . This suggests that the efficient charge transfer was further assisted by the increased conductivity with C-NWs. The addition of C-NWs improved the charge carrier density; so it is proposed that the C-NWs promote electron transfer between CB of  $\text{Cu}_2\text{O}$  and CB of  $\text{TiO}_2$ , enhancing the separation of photogenerated electron-hole pairs. Overall, the introduction of C-NWs in the nanocomposite of C-NWs/ $\text{TiO}_2$ / $\text{Cu}_2\text{O}$  enhances the PEC performance, increases charge transport, and the nanocomposite increases photostability and extends the light absorption region.

## 4. Conclusions

In summary, we fabricated a C-NW/ $\text{TiO}_2$  NF/ $\text{Cu}_2\text{O}$  heterojunction nanocomposite *via* a hydrothermal treatment and subsequent solution phase method, which provided an intimate contact between 1D  $\text{TiO}_2$  NF and  $\text{Cu}_2\text{O}$  nanocubes surrounded by C-NWs. The carbon content in the prepared samples was confirmed by both TGA and Raman spectroscopy, and DRUVS



indicated that C-NWs have strong absorption properties as there was superior absorption at higher wavelengths. C-NW/TiO<sub>2</sub> NF/Cu<sub>2</sub>O recorded enhanced PEC activity with higher photocurrent density, and impedance spectra illustrated less charge transfer resistance than bare TiO<sub>2</sub> NF and Cu<sub>2</sub>O. After calculating the charge carrier densities of TiO<sub>2</sub> NF and C-NW/TiO<sub>2</sub> NF, it was shown that the addition of C-NWs improved the charge carrier density by promoting electron transfer. Therefore, C-NW/TiO<sub>2</sub> NF/Cu<sub>2</sub>O provided superior light absorption properties, efficient charge transfer, separation of electron-hole pairs and the integration of C-NWs, which promote further electron transport within the heterojunction nanocomposite. All these properties contribute towards fabricating a nanocomposite with superior PEC activity. This work is an example of designing and fabricating effective heterojunction nanocomposite materials for solar water splitting.

## Conflicts of interest

There are no conflicts of interest to declare.

## Acknowledgements

This research was supported by the European Commission H2020 Marie S Curie Research and Innovation Staff Exchange (RISE) award (Grant No. 871998).

## References

- 1 S. Li, C. Wang, M. Cai, F. Yang, Y. Liu, J. Chen, P. Zhang, X. Li and X. Chen, Facile fabrication of TaON/Bi<sub>2</sub>MoO<sub>6</sub> core-shell S-scheme heterojunction nanofibers for boosting visible-light catalytic levofloxacin degradation and Cr(VI) reduction, *Chem. Eng. J.*, 2022, **428**, 131158, DOI: [10.1016/j.cej.2021.131158](https://doi.org/10.1016/j.cej.2021.131158).
- 2 S. Li, J. Chen, S. Hu, H. Wang, W. Jiang and X. Chen, Facile construction of novel Bi<sub>2</sub>WO<sub>6</sub>/Ta<sub>3</sub>N<sub>5</sub> Z-scheme heterojunction nanofibers for efficient degradation of harmful pharmaceutical pollutants, *Chem. Eng. J.*, 2020, **402**, 126165, DOI: [10.1016/j.cej.2020.126165](https://doi.org/10.1016/j.cej.2020.126165).
- 3 C. Wang, S. Li, M. Cai, R. Yan, K. Dong, J. Zhang and Y. Liu, Rationally designed tetra (4-carboxyphenyl) porphyrin/graphene quantum dots/bismuth molybdate Z-scheme heterojunction for tetracycline degradation and Cr(VI) reduction: Performance, mechanism, intermediate toxicity appraisal, *J. Colloid Interface Sci.*, 2022, **619**, 307–321, DOI: [10.1016/j.jcis.2022.03.075](https://doi.org/10.1016/j.jcis.2022.03.075).
- 4 S. Li, C. Wang, Y. Liu, M. Cai, Y. Wang, H. Zhang, Y. Guo, W. Zhao, Z. Wang and X. Chen, Photocatalytic degradation of tetracycline antibiotic by a novel Bi<sub>2</sub>Sn<sub>2</sub>O<sub>7</sub>/Bi<sub>2</sub>MoO<sub>6</sub> S-scheme heterojunction: Performance, mechanism insight and toxicity assessment, *Chem. Eng. J.*, 2022, **429**, 132519, DOI: [10.1016/j.cej.2021.132519](https://doi.org/10.1016/j.cej.2021.132519).
- 5 S. Li, C. Wang, M. Cai, Y. Liu, K. Dong and J. Zhang, Designing oxygen vacancy mediated bismuth molybdate (Bi<sub>2</sub>MoO<sub>6</sub>)/N-rich carbon nitride (C<sub>3</sub>N<sub>5</sub>) S-scheme heterojunctions for boosted photocatalytic removal of tetracycline antibiotic and Cr(VI): Intermediate toxicity and mechanism insight, *J. Colloid Interface Sci.*, 2022, **624**, 219–232, DOI: [10.1016/j.jcis.2022.05.151](https://doi.org/10.1016/j.jcis.2022.05.151).
- 6 S. Li, M. Cai, Y. Liu, J. Zhang, C. Wang, S. Zang, Y. Li, P. Zhang and X. Li, In situ construction of a C<sub>3</sub>N<sub>5</sub> nanosheet/Bi<sub>2</sub>WO<sub>6</sub> nanodot S-scheme heterojunction with enhanced structural defects for the efficient photocatalytic removal of tetracycline and Cr(VI), *Inorg. Chem. Front.*, 2022, **9**, 2479–2497, DOI: [10.1039/D2QI00317A](https://doi.org/10.1039/D2QI00317A).
- 7 C. Wang, M. Cai, Y. Liu, F. Yang, H. Zhang, J. Liu and S. Li, Facile construction of novel organic–inorganic tetra (4-carboxyphenyl) porphyrin/Bi<sub>2</sub>MoO<sub>6</sub> heterojunction for tetracycline degradation: Performance, degradation pathways, intermediate toxicity analysis and mechanism insight, *J. Colloid Interface Sci.*, 2022, **605**, 727–740, DOI: [10.1016/j.jcis.2021.07.137](https://doi.org/10.1016/j.jcis.2021.07.137).
- 8 J. Luo, P. Lin, P. Zheng, X. Zhou, X. Ning, L. Zhan, Z. Wu, X. Liu and X. Zhou, In situ constructing S-scheme FeOOH/MgIn<sub>2</sub>S<sub>4</sub> heterojunction with boosted interfacial charge separation and redox activity for efficiently eliminating antibiotic pollutant, *Chemosphere*, 2022, **298**, 134297, DOI: [10.1016/j.chemosphere.2022.134297](https://doi.org/10.1016/j.chemosphere.2022.134297).
- 9 J. Luo, X. Zhou, F. Yang, X. Ning, L. Zhan, Z. Wu and X. Zhou, Generating a captivating S-scheme CuBi<sub>2</sub>O<sub>4</sub>/CoV<sub>2</sub>O<sub>6</sub> heterojunction with boosted charge spatial separation for efficiently removing tetracycline antibiotic from wastewater, *J. Clean. Prod.*, 2022, **357**, 131992, DOI: [10.1016/j.jclepro.2022.131992](https://doi.org/10.1016/j.jclepro.2022.131992).
- 10 J. Luo, J. Chen, X. Chen, X. Ning, L. Zhan and X. Zhou, Construction of cerium oxide nanoparticles immobilized on the surface of zinc vanadate nanoflowers for accelerated photocatalytic degradation of tetracycline under visible light irradiation, *J. Colloid Interface Sci.*, 2021, **587**, 831–844, DOI: [10.1016/j.jcis.2020.11.044](https://doi.org/10.1016/j.jcis.2020.11.044).
- 11 A. L. Linsebigler, G. Lu and J. T. Yates, Photocatalysis on TiO<sub>2</sub> Surfaces: Principles, Mechanisms, and Selected Results, *Chem. Rev.*, 1995, **95**, 735–758, DOI: [10.1021/cr00035a013](https://doi.org/10.1021/cr00035a013).
- 12 Ü. Özgür, Y. I. Alivov, C. Liu, A. Teke, M. A. Reshchikov, S. Doğan, V. Avrutin, S.-J. Cho and H. Morkoç, A comprehensive review of ZnO materials and devices, *J. Appl. Phys.*, 2005, **98**, 041301, DOI: [10.1063/1.1992666](https://doi.org/10.1063/1.1992666).
- 13 K. Sivula, F. Le Formal and M. Grätzel, Solar Water Splitting: Progress Using Hematite (α-Fe<sub>2</sub>O<sub>3</sub>) Photoelectrodes, *ChemSusChem*, 2011, **4**, 432–449, DOI: [10.1002/cssc.201000416](https://doi.org/10.1002/cssc.201000416).
- 14 A. Kudo, K. Omori and H. Kato, A Novel Aqueous Process for Preparation of Crystal Form-Controlled and Highly Crystalline BiVO<sub>4</sub> Powder from Layered Vanadates at Room Temperature and Its Photocatalytic and Photophysical Properties, *J. Am. Chem. Soc.*, 1999, **121**, 11459–11467, DOI: [10.1021/ja992541y](https://doi.org/10.1021/ja992541y).
- 15 M. Ni, M. K. H. Leung, D. Y. C. Leung and K. Sumathy, A review and recent developments in photocatalytic water-splitting using TiO<sub>2</sub> for hydrogen production, *Renew. Sustain. Energy Rev.*, 2007, **11**, 401–425, DOI: [10.1016/j.rser.2005.01.009](https://doi.org/10.1016/j.rser.2005.01.009).



- 16 R. Abe, Recent progress on photocatalytic and photoelectrochemical water splitting under visible light irradiation, *J. Photochem. Photobiol., C*, 2010, **11**, 179–209, DOI: [10.1016/j.jphotochemrev.2011.02.003](#).
- 17 M. Hara, T. Kondo, M. Komoda, S. Ikeda, J. N. Kondo, K. Domen, M. Hara, K. Shinohara and A. Tanaka, Cu<sub>2</sub>O as a photocatalyst for overall water splitting under visible light irradiation, *Chem. Commun.*, 1998, 357–358, DOI: [10.1039/a707440i](#).
- 18 S. J. A. Moniz, S. A. Shevlin, D. J. Martin, Z.-X. Guo and J. Tang, Visible-light driven heterojunction photocatalysts for water splitting – a critical review, *Energy Environ. Sci.*, 2015, **8**, 731–759, DOI: [10.1039/C4EE03271C](#).
- 19 K. Sekar, C. Chuaicham, B. Vellaichamy, W. Li, W. Zhuang, X. Lu, B. Ohtani and K. Sasaki, Cubic Cu<sub>2</sub>O nanoparticles decorated on TiO<sub>2</sub> nanofiber heterostructure as an excellent synergistic photocatalyst for H<sub>2</sub> production and sulfamethoxazole degradation, *Appl. Catal. B Environ.*, 2021, **294**, 120221, DOI: [10.1016/j.apcatb.2021.120221](#).
- 20 K. Woan, G. Pyrgiotakis and W. Sigmund, Photocatalytic Carbon-Nanotube-TiO<sub>2</sub> Composites, *Adv. Mater.*, 2009, **21**, 2233–2239, DOI: [10.1002/adma.200802738](#).
- 21 W. Li, Y. Bai, C. Liu, Z. Yang, X. Feng, X. Lu, N. K. van der Laak and K.-Y. Chan, Highly Thermal Stable and Highly Crystalline Anatase TiO<sub>2</sub> for Photocatalysis, *Environ. Sci. Technol.*, 2009, **43**, 5423–5428, DOI: [10.1021/es8037005](#).
- 22 W. Li, Y. Bai, W. Liu, C. Liu, Z. Yang, X. Feng, X. Lu and K.-Y. Chan, Single-crystalline and reactive facets exposed anatase TiO<sub>2</sub> nanofibers with enhanced photocatalytic properties, *J. Mater. Chem.*, 2011, **21**, 6718, DOI: [10.1039/c1jm10115c](#).
- 23 S. Karthikeyan, S. Kumar, L. J. Durndell, M. A. Isaacs, C. M. A. Parlett, B. Coulson, R. E. Douthwaite, Z. Jiang, K. Wilson and A. F. Lee, Size-Dependent Visible Light Photocatalytic Performance of Cu<sub>2</sub>O Nanocubes, *ChemCatChem*, 2018, **10**, 3554–3563, DOI: [10.1002/cctc.201800439](#).
- 24 M. Amjad, M. Iqbal, A. Faisal, A. M. Junjua, I. Hussain, S. Z. Hussain, H. A. Ghramh, K. A. Khan and H. A. Janjua, Hydrothermal synthesis of carbon nanodots from bovine gelatin and PHM3 microalgae strain for anticancer and bioimaging applications, *Nanoscale Adv.*, 2019, **1**, 2924–2936, DOI: [10.1039/C9NA00164F](#).
- 25 Q. Cui, F. He, X. Wang, B. Xia and L. Li, Gold Nanoflower@Gelatin Core-Shell Nanoparticles Loaded with Conjugated Polymer Applied for Cellular Imaging, *ACS Appl. Mater. Interfaces*, 2013, **5**, 213–219, DOI: [10.1021/am302589g](#).
- 26 Q. Liang, W. Ma, Y. Shi, Z. Li and X. Yang, Easy synthesis of highly fluorescent carbon quantum dots from gelatin and their luminescent properties and applications, *Carbon N. Y.*, 2013, **60**, 421–428, DOI: [10.1016/j.carbon.2013.04.055](#).
- 27 H. G. Yang, G. Liu, S. Z. Qiao, C. H. Sun, Y. G. Jin, S. C. Smith, J. Zou, H. M. Cheng and G. Q. Lu, Solvothermal Synthesis and Photoreactivity of Anatase TiO<sub>2</sub> Nanosheets with Dominant {001} Facets, *J. Am. Chem. Soc.*, 2009, **131**, 4078–4083, DOI: [10.1021/ja808790p](#).
- 28 S. Sun, X. Zhang, X. Song, S. Liang, L. Wang and Z. Yang, Bottom-up assembly of hierarchical Cu<sub>2</sub>O nanospheres: controllable synthesis, formation mechanism and enhanced photochemical activities, *CrystEngComm*, 2012, **14**, 3545, DOI: [10.1039/c2ce25071c](#).
- 29 S. Zhang, H. Liu, C. Sun, P. Liu, L. Li, Z. Yang, X. Feng, F. Huo and X. Lu, CuO/Cu<sub>2</sub>O porous composites: shape and composition controllable fabrication inherited from metal organic frameworks and further application in CO oxidation, *J. Mater. Chem. A.*, 2015, **3**, 5294–5298, DOI: [10.1039/C5TA00249D](#).
- 30 M. Hiramatsu and M. Hori, *Carbon Nanowalls: Synthesis and Emerging Applications*, Springer Vienna, Vienna, 2010, DOI: [10.1007/978-3-211-99718-5](#).
- 31 F. Meng, J. Li, S. K. Cushing, J. Bright, M. Zhi, J. D. Rowley, Z. Hong, A. Manivannan, A. D. Bristow and N. Wu, Photocatalytic Water Oxidation by Hematite/Reduced Graphene Oxide Composites, *ACS Catal.*, 2013, **3**, 746–751, DOI: [10.1021/cs300740e](#).
- 32 J. Zhang, W. Liu, X. Wang, X. Wang, B. Hu and H. Liu, Enhanced decoloration activity by Cu<sub>2</sub>O@TiO<sub>2</sub> nanobelts heterostructures via a strong adsorption-weak photodegradation process, *Appl. Surf. Sci.*, 2013, **282**, 84–91, DOI: [10.1016/j.apsusc.2013.05.054](#).
- 33 Y. Bessekhoud, D. Robert and J.-V. Weber, Photocatalytic activity of Cu<sub>2</sub>O/TiO<sub>2</sub>, Bi<sub>2</sub>O<sub>3</sub>/TiO<sub>2</sub> and ZnMn<sub>2</sub>O<sub>4</sub>/TiO<sub>2</sub> heterojunctions, *Catal. Today*, 2005, **101**, 315–321, DOI: [10.1016/j.cattod.2005.03.038](#).
- 34 S. G. Babu, R. Vinoth, D. Praveen Kumar, M. V. Shankar, H.-L. Chou, K. Vinodgopal and B. Neppolian, Influence of electron storing, transferring and shuttling assets of reduced graphene oxide at the interfacial copper doped TiO<sub>2</sub> p-n heterojunction for increased hydrogen production, *Nanoscale*, 2015, **7**, 7849–7857, DOI: [10.1039/C5NR00504C](#).
- 35 J. Hou, C. Yang, H. Cheng, S. Jiao, O. Takeda and H. Zhu, High-performance p-Cu<sub>2</sub>O/n-TaON heterojunction nanorod photoanodes passivated with an ultrathin carbon sheath for photoelectrochemical water splitting, *Energy Environ. Sci.*, 2014, **7**, 3758–3768, DOI: [10.1039/C4EE02403F](#).
- 36 S. Li, C. Wang, Y. Liu, B. Xue, W. Jiang, Y. Liu, L. Mo and X. Chen, Photocatalytic degradation of antibiotics using a novel Ag/Ag<sub>2</sub>S/Bi<sub>2</sub>MoO<sub>6</sub> plasmonic p-n heterojunction photocatalyst: Mineralization activity, degradation pathways and boosted charge separation mechanism, *Chem. Eng. J.*, 2021, **415**, 128991, DOI: [10.1016/j.cej.2021.128991](#).
- 37 S. Sakthivel and H. Kisch, Daylight Photocatalysis by Carbon-Modified Titanium Dioxide, *Angew. Chem., Int. Ed.*, 2003, **42**, 4908–4911, DOI: [10.1002/anie.200351577](#).
- 38 R. A. Parker, Static Dielectric Constant of Rutile (TiO<sub>2</sub>), 1.6–106 K, *Phys. Rev.*, 1961, **124**, 1719–1722, DOI: [10.1103/PhysRev.124.1719](#).
- 39 Z. Zhang and P. Wang, Highly stable copper oxide composite as an effective photocathode for water splitting via a facile electrochemical synthesis strategy, *J. Mater. Chem.*, 2012, **22**, 2456–2464, DOI: [10.1039/C1JM14478B](#).
- 40 A. Paracchino, J. C. Brauer, J.-E. Moser, E. Thimsen and M. Graetzel, Synthesis and Characterization of





- High-Photoactivity Electrodeposited Cu<sub>2</sub>O Solar Absorber by Photoelectrochemistry and Ultrafast Spectroscopy, *J. Phys. Chem. C.*, 2012, **116**, 7341–7350, DOI: [10.1021/jp301176y](https://doi.org/10.1021/jp301176y).
- 41 M. Wang, L. Sun, Z. Lin, J. Cai, K. Xie and C. Lin, p–n Heterojunction photoelectrodes composed of Cu<sub>2</sub>O-loaded TiO<sub>2</sub> nanotube arrays with enhanced photoelectrochemical and photoelectrocatalytic activities, *Energy Environ. Sci.*, 2013, **6**, 1211, DOI: [10.1039/c3ee24162a](https://doi.org/10.1039/c3ee24162a).
- 42 Y. Hou, X. Y. Li, Q. D. Zhao, X. Quan and G. H. Chen, Fabrication of Cu<sub>2</sub>O/TiO<sub>2</sub> nanotube heterojunction arrays and investigation of its photoelectrochemical behavior, *Appl. Phys. Lett.*, 2009, **95**, 093108, DOI: [10.1063/1.3224181](https://doi.org/10.1063/1.3224181).

